NASA TECHNICAL NOTE

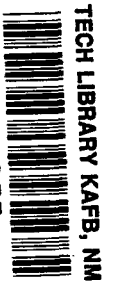

MOTION OF SINGLE BUBBLES UNDER LOW GRAVITATIONAL CONDITIONS

by John B. Haggard, Jr., and William J. Masica

Lewis Research Center

Cleveland, Ohio

NATIONAL AERONAUTICS AND SPACE ADMINISTRATION • WASHINGTON, D. C. • OCTOBER 1969

1. Report No. NASA TN D-5462	2. Government Accession No.	3. Recipient's Catalog No.
4. Title and Subtitle MOTION OF SINGLE BUBBLES UNDER LOW GRAVITATIONAL CONDITIONS		5. Report Date October 1969 6. Performing Organization Code
7. Author(s) John B. Haggard, Jr., and William J. Masica		8. Performing Organization Report No. E-5128
9. Performing Organization Name and Address Lewis Research Center National Aeronautics and Space Administration Cleveland, Ohio 44135		10. Work Unit No. 124-09 11. Contract or Grant No.
12. Sponsoring Agency Name and Address National Aeronautics and Space Administration Washington, D.C. 20546		13. Type of Report and Period Covered Technical Note 14. Sponsoring Agency Code

15. Supplementary Notes

16. Abstract

An experimental study was undertaken to examine single, noncondensable bubble motion under low-gravity conditions. These data were compared with normal-gravity theory and empirical results. The M number (a characteristic dimensionless parameter containing gravity and the liquid properties) was found to be a significant parameter in correlating normal- and low-gravity data. This report, together with normal-gravity theory, predicts bubble shape and terminal velocity when the liquid properties, the bubble volume, and the applied gravity field are known. The results are applicable to a range of spherical and ellipsoidal bubbles with Reynolds numbers above 50.

17. Key Words *(Suggested by Author(s))* Bubbles Low gravity Weightlessness Two-phase flow	18. Distribution Statement Unclassified - unlimited

19. Security Classif. (of this report)	20. Security Classif. (of this page)	21. No. of Pages	22. Price*
Unclassified	Unclassified	31	$3.00

*For sale by the Clearinghouse for Federal Scientific and Technical Information
Springfield, Virginia 22151

MOTION OF SINGLE BUBBLES UNDER LOW GRAVITATIONAL CONDITIONS

by John B. Haggard, Jr., and William J. Masica

Lewis Research Center

SUMMARY

An experimental study was undertaken to examine single, noncondensable bubble motion under low-gravity conditions. These data were compared with normal-gravity theory and empirical results. The M number (a characteristic dimensionless parameter containing gravity and the liquid properties) was found to be a significant parameter in correlating normal- and low-gravity data. This report, together with normal-gravity theory, predicts bubble shape and terminal velocity when the liquid properties, the bubble volume, and the applied gravity field are known. The results are applicable to a range of spherical and ellipsoidal bubbles with Reynolds numbers above 50.

INTRODUCTION

Small gas bubbles may form in the liquid systems of space vehicles. The dynamics of these bubbles can be an important consideration in vehicle design. Bubbles may be formed, for example, by liquid boiling at sources of large heat input or by vehicle maneuvers that result in turbulent liquid motion such as sloshing and reorientation. The ensuing bubble dynamics must be known and accounted for, as the performance of liquid space vehicle systems can be affected by the presence of entrained gas bubbles.

In general, the terminal velocities of gas bubbles are gravity-dependent. The general problem involving clusters of bubbles in a nonequilibrium thermal environment is complicated by the processes of condensation, breakup, and coalescence. Some of these processes have been studied with regard to space vehicle liquid systems under low-gravity conditions; for example, by Welch and Funk (ref. 1), Holister, Satterlee, and Cohan (ref. 2), and Blackmon (refs. 3 and 4). Understanding the distribution and dynamics of clusters of bubbles presumes a knowledge of the dynamics of a single bubble. Some low-gravity experimental data on the velocity of nucleate bubbles after they are detached from a heated surface were obtained by Siegel (ref. 5). However, no other

low-gravity experimental data on single-bubble motion are available.

Because the literature on bubble dynamics under normal-gravity conditions is so extensive, no attempt will be made to summarize the numerous papers applicable to the subject. An excellent summary and comprehensive reference list are given in a recent book by Brodkey (ref. 6). The papers of the experimentalists Haberman and Morton (ref. 7) and Peebles and Garber (ref. 8), and the theoretical work of Chao (ref. 9) and Moore (refs. 10 to 12) are frequently cited for their studies on the dynamics of single, noncondensable gas bubbles.

This report presents the results of an experimental study of some basic aspects of the motion of single, noncondensable gas bubbles under low-gravity conditions, and compares these results with published theory and experimental results. It is presently only surmised that the theory and empirical results based on normal-gravity theory can be scaled to low-gravity environments. The study was conducted in the Lewis Research Center's 2.2-Second Zero-Gravity Facility. The Facility provided gravity levels from 0.005 to 0.05 g. Bubble radii ranged from 0.07 to 0.43 centimeter. Data were acquired on the terminal velocity and shape of these bubbles for Reynolds numbers from 12 to 1030.

SYMBOLS

a	acceleration, cm/sec^2
C_D	drag coefficient, $8r_{eq}a/3v^2$
$G(\chi)$	dimensionless function of distortion parameter obtained by Moore (ref. 6)
g	acceleration due to gravity, 980 cm/sec^2
$H(\chi)$	dimensionless function of distortion parameter
M	dimensionless parameter, $\eta^4 a/\rho\sigma^3$
Re	Reynolds number, $2r_{eq}v/\nu$
r_{eq}	equivalent radius of spherical bubble of same volume as an observed bubble, cm
r_h	semimajor axis perpendicular to direction of motion of bubble, cm
r_v	semiminor axis parallel to direction of motion of bubble, cm
T	temperature, ^oC
t	time, sec
V	volume of bubble, cm^3
v	terminal velocity, cm/sec

$We(\chi)$	Weber number defined in terms of distortion parameter
η	liquid viscosity, cP
ν	kinematic viscosity, η/ρ, cm^2/sec
ρ	liquid density, g/cm^3
σ	surface tension, dynes/cm
χ	distortion parameter, r_h/r_v

ANALYSIS

In an isothermal liquid the resulting terminal velocity of a bubble is governed by the force balance of bouyant and drag forces. The bouyant force is known to be equal to the weight of the volume of liquid displaced. Drag forces, in general, depend on the shape of the bubble, the size of the boundary layer around the bubble, and the physical characteristics of the wake behind the bubble. Since the size of boundary layers and wakes can be characterized in terms of the Reynolds number ($2r_{eq}v/\nu$), bubble motion may be divided into various Reynolds number regimes:

(1) At small Reynolds numbers ($Re < 1$) the boundary layer is essentially infinite, there is no wake behind the bubble, and the bubble is of fixed spherical shape. The solution to this problem proposed by Hadamard and Rybczynski (and discussed in ref. 7) parallels the creeping flow solution that yields Stokes law for solid spheres. The primary difference is that the surface of the bubble cannot support any stress.

(2) For Reynolds numbers greater than 1 and up to the point at which the bubble distorts, the boundary layer is decreasing with increasing Reynolds number. The dissipation of energy due to the viscous forces in the boundary layer around the bubble is the principal cause of drag. Representative solutions to this problem are those of Chao (ref. 9) and Moore (refs. 10 to 12). The primary differences in their solutions is in their treatment of the internal circulation of the gas inside the bubble.

(3) In the regime where the bubble distorts, the motion depends on the degree of distortion. Moore (ref. 12) suggests a solution for this regime in which the M number ($\eta^4 a/\rho\sigma^3$) is a correlating parameter. This dimensionless grouping is related to the change in pressure across the bubble and the fluid properties (ref. 7). Bubbles in this regime will always be oblate ellipsoids. Before the drag can be determined, the changing bubble shape, the boundary layer, and the wake must be accounted for.

This report is concerned with bubbles in the latter two regimes. Since many theories have been published as solutions to the motion in these regimes, we selected one, a theory proposed by Moore, as representative of a class of normal-gravity solutions. Moore specifically uses the M number as a correlating parameter and appears to have

the most complete theory in the distorted gas bubble regime. His theory, which is applicable to liquids and test conditions where the M number is less than 10^{-8}, extends from Reynolds numbers greater than 50 to the point where the bubble is distorted such that the ratio of the major axis to minor axis of the bubble equals 4. This ratio is the distortion parameter χ, where

$$\chi = \frac{r_h}{r_v} \tag{1}$$

This distortion parameter for a spherical bubble equals 1; for oblate ellipsoidal bubbles, it is greater than 1.

Moore's solution considers the dissipation of energy in the boundary layer and the energy loss in the wake. The drag on the bubble is calculated as a result of these energy losses. The drag force may be expressed in the form

$$\text{Drag} = \frac{1}{2}\rho\pi r_{eq}^2 C_D v^2 \tag{2}$$

where r_{eq} has the physical meaning of the radius of an imagined spherical bubble containing the same volume as the observed bubble. This form of the drag differs from the standard, aerodynamic usage, where the frontal area perpendicular to the flow, not πr_{eq}^2, would be used. As a result the drag coefficient in equation (2) is dependent on the shape of the bubble. For ellipsoids the equivalent radii r_{eq} can be calculated from the equation

$$r_{eq} = \left(r_v r_h^2\right)^{1/3} \tag{3}$$

The drag coefficient is the term which takes into account all of the various mechanisms for dissipating energy. The drag coefficient is, in general, a function of the Reynolds number. Moore's solution defines the drag coefficient in terms of the Reynolds number and various functions of χ, a parameter which takes into account the shape of the bubble. The solution is

$$C_D = \frac{48G(\chi)}{Re}\left[1 + \frac{H(\chi)}{Re^{1/2}}\right] \tag{4}$$

where

$$G(\chi) = \frac{1}{3}\chi^{4/3}(\chi^2 - 1)^{3/2}\frac{(\chi^2 - 1)^{1/2} - (2 - \chi^2)\sec^{-1}(\chi)}{\left[\chi^2\sec^{-1}(\chi) - (\chi^2 - 1)^{1/2}\right]^2}$$

and $H(\chi)$ is a dimensionless parameter found by Moore (ref. 12) who obtained it by numerical integration, and for convenience is listed in table I. By equating the drag and buoyant forces, a solution for C_D may be determined in dimensionless form as

$$C_D = \frac{4}{3}\mathrm{Re}^4\mathrm{We}(\chi)^{-3}M \tag{5}$$

where $\mathrm{We}(\chi)$ has the numerical value of the Weber number and is given by

$$\mathrm{We}(\chi) = 4\chi^{-4/3}(\chi^3 + \chi - 2)\frac{\left[\chi^2\sec^{-1}(\chi) - (\chi^2 - 1)^{1/2}\right]^2}{(\chi^2 - 1)^3}$$

When a value of χ and an M number are chosen, equations (4) and (5) can be solved simultaneously for C_D and Re. The APPENDIX presents techniques for solving these equations.

The result of this effort is to generate a curve of C_D as a function of Reynolds number. These results can be shown in terms of terminal velocity v as a function of equivalent radius r_{eq} by means of the transformation equations

$$v = \left(\frac{4}{3}\frac{a\mathrm{Re}\nu}{C_D}\right)^{1/3} \tag{6}$$

$$r_{eq} = \left(\frac{3}{32}\frac{\nu^2}{a}\mathrm{Re}^2 C_D\right)^{1/3} \tag{7}$$

The transformation equations (6) and (7) were found from both the definition of the Reynolds number and an equation for the drag coefficient found by equating the drag and buoyant forces.

These results indicate that the C_D-Re curve is a universal one for a given M number, and not merely a curve for one test liquid. By the transformation equations, a given M-number curve in the C_D-Re plane may have many possible curves in the v-r_{eq} plane. This is due to different test liquid properties and gravity fields, all of which go

into making up a fixed M number. Changing the M number will of course, change the C_D-Re curve.

The M number, for a series of test liquids, can be varied by changing the gravity level on the experiment and studying the drag characteristics (with Reynolds number) of the motion of bubbles. This procedure should show whether the M number is the proper parameter for scaling normal-gravity results to low-gravity environments. The experiment should include a study of the motion of bubbles in the ellipsoidal region since it is here that the M number is predicted to play an important role in determining bubble motion.

APPARATUS AND PROCEDURE

Test Liquids

The liquids used in this study were 1-butanol, anhydrous ethanol, and methanol. All were analytic reagent-grade liquids. Handbook values for the three pertinent liquid properties (density, viscosity, and surface tension) at specific temperatures for each of the three test liquids are given in table II. These properties were used in the calculations of the Reynolds number ($2r_{eq}v/\nu$) and the M number ($\eta^4 a/\rho\sigma^3$). Kinematic viscosity and the liquid property ratio $\eta^4/\rho\sigma^3$ are plotted in figure 1 as functions of temperature. Both the Reynolds number and the M number for each test was temperature-corrected. The investigation was limited to low-viscosity (0.5 to 3.0 cP) liquids, because bubbles in these liquids exhibit larger, more easily observable, terminal velocities.

Low-Gravity Tests

Test facility. - The experimental tests were conducted in the zero-gravity facility shown in figure 2. The free-fall distance of 24 meters allowed a 2.2-second period of weightless test time. Effects of air drag on the experiment were maintained below 10^{-5} g by allowing the experiment package to fall inside a drag shield. During the drop, the package and drag shield fell simultaneously but were independent of each other. Low gravity was achieved on the experiment package by means of a gas thruster. At the conclusion of the drop, the package was decelerated by the penetration of the drag shield spikes in the sand of the deceleration container.

Experiment package. - The experiment tank was mounted in the experiment package shown in figure 3. The experiment package contained a high-speed, 16-millimeter, motion-picture camera and backlighting, which was used to provide uniform illumination. A digital clock, accurate to 0.01 second, was in the field of view of the camera. Both

the calibration of the magnitude of the thruster, used to apply a low-gravity acceleration, and alinement of the package's center of mass through the thrust axis, was performed according to the procedure outlined in reference 13.

Experiment tank. - The acrylic plastic tank (fig. 4) used in low-gravity tests was made square in cross section to provide flat faces to make refraction negligible. The tank dimensions are 17.8 by 9.3 by 9.3 centimeters. The insert at the top of the tank was designed with an apex in it to provide an initial position for the vapor bubbles and contained a reservoir filled with the test liquid, with fill-vent lines extending down into the tank. The reservoir provided an expansion volume to prevent either bubble collapse or unwanted vapor being pulled into the fill-vent lines whenever the tank heated or cooled slightly. The cross section of the tank used in this study was large enough so that wall effects were negligible. Wall effects are treated in reference 14, where it was found that they were negligible whenever the ratio of tank diameter to bubble diameter is greater than 10. That ratio for the test runs ranged from 10 to 60. A scale with 0.2-centimeter divisions was mounted vertically at the same distance from the camera as the path of the bubble. For some of the tests, two tanks were studied side by side.

Operating procedure. - Prior to all tests, the tank was ultrasonically cleaned in a mild detergent solution, rinsed in distilled water, rinsed again in pure methanol, and dried in warm filtered air. This procedure was followed to prevent the tank from contaminating the test liquid. The tank was filled with liquid and a measured amount of air was injected into the tank, with a microliter syringe, through the fill-vent lines. The resulting bubble was located at the apex of the tank. Two seconds before the drop, the camera and lights were turned on; when the supporting music wire was cut, the clock started. After the package fell for about 0.2 second, the thruster started and remained on for the balance of the drop. The sequential position of the experiment package in the drag shield during the test drop is shown in figure 5. The temperature of the liquid was recorded within 5 minutes after the drop. An isothermal condition was assumed for the system during the drop.

Normal-Gravity Tests

The tank used in normal-gravity tests is shown in figure 6. It had a square cross section 5.6 by 5.6 centimeters and is 17.8 centimeters high. The ratio of tank diameter to bubble diameter ranged from 17 to 83, hence, wall effects were negligible. Prior to each test, the tank was also ultrasonically cleaned and filled with liquid. With a microliter syringe, a measured amount of air was injected into the tube that extended from the bottom of the tank. The bubble moved along the length of the tube and eventually into the tank.

As the bubble rose in the tank it was photographed with a high-speed camera. The temperature was recorded just prior to the test.

RESULTS AND DISCUSSION

Representative Data

Bubble velocity and bubble shape measurements were obtained from the motion-picture film of each test. A typical low-gravity test is shown in figure 7. The double tanks used in the particular run shown were both filled with ethanol. The acceleration was 9.8 centimeters per second squared. The left-hand tank has a 0.23-centimeter-radius bubble traveling at 6.3 centimeters per second, the right-hand tank has a 0.18-centimeter-radius bubble at a terminal velocity of 4.8 centimeters per second. At the time of application of the thrust, each bubble had detached from the apex of the tank, was located on the centerline of the tank, and had a near-zero velocity. Radial oscillations of the bubble, which commonly occur as the bubble detaches from the top of the tank, damped out rapidly. After the thrust was applied, the bubble began moving. About midway into the test, the bubble had reached terminal velocity and remained at this velocity until the end of the test. Its terminal velocity was measured over an average distance of 5 to 10 bubble diameters. Typically, terminal velocity measurements took place within 1 second.

The time and distance the bubbles traveled were recorded at intervals throughout the test. After a judgement of when terminal velocity was reached, the slope of the least-mean-square fit to the remaining points was considered to be the terminal velocity of the bubble (see fig. 8). After each bubble had reached terminal velocity, the shape measurements were made. The shape was determined by measuring the horizontal and vertical axes of the bubble and computing χ, the distortion parameter. Bubbles were considered to be spherical if $0.9 \leq \chi \leq 1.05$, because of the inherent inaccuracies in the measurements of the bubble axes, particularly around $\chi = 1$. The bubbles observed at terminal velocity appeared to be fixed in shape with no radial oscillations. Distorted bubbles, photographed in runs using single tanks, are shown in figure 9. The single tanks allowed more precise measurements of the shape of the bubble.

The drag coefficient C_D was determined from the experimental data and the equation

$$C_D = \frac{8 r_{eq} a}{3 v^2} \tag{8}$$

which is found by rearranging equation (6).

This is a standard form for the experimental drag coefficient of a bubble (ref. 7).

Comparison of Low-Gravity Data With Normal-Gravity Data and Theory

A summary of the experimental results of this study is found in table III. Reynolds numbers ranged from 12 to 1030 and the distortion parameter ranged from 1.0 to about 2.6. In low-gravity tests, only rectilinear motion was observed. This is a distinctly different behavior than in normal gravity, where two types of motion were observed. At small Reynolds numbers, rectilinear motion occurred, while at high Reynolds numbers (of the order of several hundred) helical motion was observed.

Gravity dependence. - The effect of a change in the gravity field on the terminal velocity of a bubble is shown in figure 10. Included in these figures are data taken by Haberman and Morton (ref. 7) and Peebles and Garber (ref. 8). The trend in the data is nearly the same at each gravity level, but the data are shifted to lower terminal velocities and larger equivalent radii. Where the terminal velocity appears relatively independent of the equivalent radius, it is known that the velocity depends on gravity to the 1/4 power (ref. 5). At smaller equivalent radii, where the slope of the velocity-versus-radius data is approximately 2, the terminal velocity depends on gravity to the first power (ref. 7). The change in gravity dependence occurs near those radii where the bubble distorts. The shift of the low-gravity data in figure 10 shows that the gravity-dependence cannot be scaled directly from a knowledge of the velocity and equivalent radius only. Some other parameter must also be important.

Comparison of theory with data. - Moore's solution, as described in the ANALYSIS section, and the data from table III were used to see how well a representative solution correlated to low-gravity results. The only consideration of gravity that occurred in the solution was contained in the M number. The capability of the experiment to allow changes in the gravity level gave a wide range to the M number for a given test liquid.

The same data that were displayed in figure 10 in the terminal velocity - equivalent radius plane are displayed in figure 11 in the drag coefficient - Reynolds number plane. Moore's theoretical curves, which are explicitly dependent on M number, are shown for normal gravity and low gravity by solid and dashed lines, respectively. The data in figure 11 are over an M-number range of more than 10^4 at accelerations between 1 and 0.016 g. It is seen that Moore's theory is in fair agreement with the data over this range and that the M number can be used as a scaling parameter for low-gravity conditions.

Moore's theory also predicts the distortion parameter of the bubble for a liquid at a certain M number as a function of its equivalent radius. Distortion occurs near that point where the drag coefficient is a minimum. The functional dependence of

χ on the equivalent radius is shown in figure 12. The figure shows that Moore has reasonably predicted the distortion of a bubble within the limits of the experiment. It can be noted from figure 12 that, in low-gravity, the shape of the bubble distorts from a sphere to an oblate ellipsoid at much larger bubble radii than at normal gravity. The rate of distortion with increasing bubble size was observed to be much less in low gravity. These results are in agreement with Moore's theory.

The data obtained at NASA and from the normal-gravity experimenters (refs. 7 and 8) are shown in figure 13. The M numbers have been rounded off to the nearest half decade. Bubble distortion begins to occur near the minima of the curves. For distorted bubbles, a trend can be observed for the liquids tested. The upward shift of the curve and larger distortion of the bubble are delayed to higher Reynolds numbers and lower drag coefficients for lower-M-number test conditions. The data verify this predicted shift for an M-number range from 10^{-7} to 10^{-13}. The absolute value of the data in the various M-number regimes as compared with Moore's theory shows a larger error as the M number is decreased.

Application. - It is possible to predict the terminal velocity of a bubble and its shape as functions of the bubble size, given the liquid properties and the applied gravity field. This is done by first determining a test M number, then generating a curve in the drag coefficient - Reynolds number plane by means of the techniques employed in the APPENDIX. This curve is then transformed point by point into the terminal velocity - equivalent radius plane by means of the parameteric equations (6) and (7). The terminal velocity can be found for various bubble volumes by knowing

$$r_{eq} = \sqrt[3]{\frac{3V}{4}} \tag{10}$$

where V is the known bubble volume.

The shape is found by using the lines where the distortion parameter is constant (see fig. 14) and equation (7). The result is a curve of distortion parameter as a function of the equivalent radius. Such a curve is shown in figure 12. The preceding methods apply to bubbles with a range of the distortion parameter less than 4 and with Reynolds numbers above 50.

SUMMARY OF RESULTS

An experimental study was undertaken to examine some basic aspects of the motion of single noncondensable bubbles under low-gravity conditions. Data were obtained on bubble shape and terminal velocity for Reynolds numbers from 12 to 1030, where bubble

radii ranged in size from 0.07 to 0.43 centimeter. The study was conducted in the Lewis Research Center's 2.2-Second Zero-Gravity Facility, which provided gravity levels from 0.005 to 0.05 g. These data were compared with normal-gravity theory and empirical results.

The following results were observed:

1. Only rectilinear motion was observed in the low-gravity tests of this study. This is a distinctly different behavior than in normal gravity, where over the same range of Reynolds numbers bubbles move in either rectilinear or helical motion, with Reynolds numbers of several hundred being the point where the change in the type of motion is observed.

2. The study showed that the terminal velocity of a bubble in low gravity is, as expected, reduced from its normal-gravity value. The percentage of this reduction varies with the size of the bubble.

3. In low gravity, because of the reduced velocity, the shape of the bubble distorted from spherical to ellipsoidal at much larger bubble radii than in normal gravity. The rate of change of distortion with increasing bubble radius was observed to be much less in low gravity.

4. Using Moore's solution as representative of a class of theoretical descriptions of bubble motion within the Reynolds number regimes studied, it was found that this solution was in fair agreement with the data when the solution was scaled by the M number. The M number ranged from 10^{-7} to 10^{-13}.

Lewis Research Center,
National Aeronautics and Space Administration,
Cleveland, Ohio, June 23, 1969,
124-09-17-01-22.

APPENDIX - COMPUTATIONAL PROCEDURES FOR MOORE'S ANALYSIS

Moore's solution defines the drag coefficient C_D in terms of the Reynolds number Re and two functions of χ, a parameter which takes into account the shape of the bubble. Strict limitations on this equation state that the Reynolds number must be above 50 and that the distortion parameter χ must be less than 2, for liquids and test conditions such that the M number is less than 10^{-8}. However, as was pointed out by Moore, the equation yields reasonable results up to $\chi = 4$. The solution that was presented in the ANALYSIS section is

$$C_D = \frac{48G(\chi)}{Re}\left[1 + \frac{H(\chi)}{Re^{1/2}}\right] \tag{4}$$

where

$$G(\chi) = \frac{1}{3}\chi^{4/3}\left(\chi^2 - 1\right)^{3/2}\frac{\left(\chi^2 - 1\right)^{1/2} - \left(2 - \chi^2\right)\sec^{-1}(\chi)}{\left[\chi^2\sec^{-1}(\chi) - \left(\chi^2 - 1\right)^{1/2}\right]^2}$$

and $H(\chi)$ is a dimensionless parameter found by Moore (ref. 12) who obtained it by numerical integration, and for convenience is listed in table I.

By equating the drag and bouyant forces, a solution for C_D was determined in dimensionless form as

$$C_D = \frac{4}{3}Re^4 We(\chi)^{-3} M \tag{5}$$

where We(x) has the numerical value of the Weber number and is given by

$$We(\chi) = 4\chi^{-4/3}\left(\chi^3 + \chi - 2\right)\frac{\left[\chi^2\sec^{-1}(\chi) - \left(\chi^2 - 1\right)^{1/2}\right]^2}{\left(\chi^2 - 1\right)^3}$$

This process of generating the C_D-Re curve for a given M number begins by assuming a value of χ. The functions, $We(\chi)$, $H(\chi)$, and $G(\chi)$ are then determined. Equations (4) and (5) are then solved simultaneously for C_D and Re. Due to the complexity of the functional relation of C_D on Re, particularly in equation (4), numerical techniques were used to calculate C_D to the nearest hundredth. Results of these compu-

tations are listed in table IV. It shows, for example, that a bubble in a liquid and a gravity field with an M_o number of 10^{-8}, which is distorted so that $\chi = 1.1$, is predicted to have a drag coefficient of 0.67 at a Reynolds number of 59.1. A graphical representation of the relation of C_D to Re for constant values of M_o number and the distortion parameter χ is shown in figure 14.

REFERENCES

1. Welch, N. E.; and Funk, E.: Distribution of Noncondensable Gases in Liquids Under Low-G Conditions. Paper presented at USAF/OSR and Lockheed Missiles and Space Co. Symposium on Fluid Mechanics and Heat Transfer Under Low Gravitational Conditions, Palo Alto, Calif., June 24-25, 1965.
2. Holister, M. P.; Satterlee, H. M.; Cohan, H.: A Study of Liquid Propellant Behavior During Periods of Varying Accelerations. Rep. LMSC-A874728, Lockheed Missiles and Space Co. (NASA CR-92082), May 23, 1967.
3. Blackmon, J. B.: Ullage Gas Distribution in Liquid Propellant Tanks After Resettling. Rep. DAC-62202, Missile and Space Systems Div., Douglas Aircraft Co., Mar. 1968.
4. Blackmon, J. B.: Propellant Settling. Rep. DAC-62263, Missile and Space Systems Div., Douglas Aircraft Co., May 1968.
5. Siegel, Robert: Effects of Reduced Gravity of Heat Transfer. Advances in Heat Transfer. Vol. 4. J. P. Hartnett and T. F. Irvine, Jr., eds., Academic Press, 1967, pp. 190-191.
6. Brodkey, Robert S.: The Phenomena of Fluid Motions. Addison-Wesley Publ. Co., 1967.
7. Haberman, W. L.; and Morton, R. K.: An Experimental Investigation of the Drag and Shape of Air Bubbles Rising in Various Liquids. Rep. 802, David W. Taylor Model Basin, Sept. 1953. (Available from DDC as AD-19377).
8. Peebles, Fred N.; and Garber, Harold J.: Studies on the Motion of Gas Bubbles in Liquids. Chem. Eng. Progr., vol. 49, no. 2, Feb. 1953, pp. 88-97.
9. Winnikow, S.; and Chao, B. T.: Droplet Motion in Purified Systems. Phys. Fluids, vol. 9, no. 1, Jan. 1966, pp. 50-61.
10. Moore, D. W.: The Rise of a Gas Bubble in a Viscous Liquid. J. Fluid Mech., vol. 6, pt. 1, July 1959, pp. 113-130.
11. Moore, D. W.: The Boundary Layer on a Spherical Gas Bubble. J. Fluid Mech., vol. 16, pt. 2, June 1963, pp. 161-176.
12. Moore, D. W.: The Velocity of Rise of Distorted Gas Bubbles in a Liquid of Small Viscosity. J. Fluid Mech., vol. 23, pt. 4, Dec. 1965, pp. 749-766.

13. Masica, William J.; and Petrash, Donald A.: Motion of Liquid-Vapor Interface in Response to Imposed Acceleration. NASA TN D-3005, 1965.

14. Uno, Seiji; and Kintner, R. C.: Effect of Wall Proximity on the Rate of Rise of Single Air Bubbles in a Quiescent Liquid. AIChE J., vol. 2, no. 3, Sept. 1956, pp. 420-425.

TABLE I. - H(χ) IN MOORE'S SOLUTION

Distortion parameter, χ	Dimensionless function of the distortion parameter, H(χ)
1.0	-2.211
1.1	-2.129
1.2	-2.025
1.3	-1.899
1.4	-1.751
1.5	-1.583
1.6	-1.394
1.7	-1.186
1.8	-.959
1.9	-.714
2.0	-.450
2.1	-.168
2.2	.131
2.3	.448
2.4	.781
2.5	1.131
2.6	1.499
2.7	1.884
2.8	2.286
2.9	2.684
3.0	3.112
3.1	3.555
3.2	4.013
3.3	4.484
3.4	4.971
3.5	5.472
3.6	5.987
3.7	6.517
3.8	7.061
3.9	7.618
4.0	8.189

TABLE II. - SUMMARY OF LIQUID PROPERTIES

Liquid	Liquid property	Temperature, °C
1-Butanol	Liquid density, g/cm^3:	
	0.813	15
	.810	20
	.806	25
	Surface tension, dynes/cm:	
	26.2	0
	24.6	20
	22.1	50
	Liquid viscosity, cP:	
	3.38	15
	2.95	20
	2.30	30
Ethanol	Liquid density, g/cm^3:	
	0.789	20
	.785	25
	.781	30
	Surface tension, dynes/cm:	
	23.6	10
	22.8	20
	21.9	30
	Liquid viscosity, cP:	
	1.47	10
	1.20	20
	1.00	30
Methanol	Liquid density, g/cm^3:	
	0.791	20
	.787	25
	.782	30
	Surface tension, dynes/cm:	
	24.5	0
	22.6	20
	20.1	50
	Liquid viscosity, cP:	
	0.60	20
	.55	25
	.51	30

TABLE III. - SUMMARY OF EXPERIMENTAL RESULTS

Liquid	Temperature, T, ^{o}C	Acceleration, a, cm/sec^2	Terminal velocity, v, cm/sec	Equivalent radius, r_{eq}, cm	Distortion parameter, χ	Reynolds number, Re	Drag coefficient, C_D	Dimensionless parameter, $M = \eta^4 a/\rho\sigma^3$
1-Butanol	26	12.0	3.7	0.21	0.94	50	0.49	4.5×10^{-10}
	25	12.1	6.9	.38	1.20	150	.26	6.9
	26	16.0	7.7	.42	1.32	200	.30	6.0
	23	32.1	2.3	.09	.97	12	1.49	1.5×10^{-9}
	22	↓	4.9	.19	1.02	55	.67	1.7
	24	↓	7.5	.23	1.09	100	.35	1.4
	26	↓	8.7	.32	1.33	180	.36	1.2
	21	↓	9.6	.43	1.61	230	.39	1.9
	22	980	9.7	.03	1.03	19	.92	5.1×10^{-8}
	21	↓	10.4	.04	1.13	24	.97	5.6
	21	↓	21.7	.07	1.52	86	.40	5.6
	22	↓	20.2	.11	2.18	130	.71	5.1
	21	↓	19.4	.17	2.36	190	1.20	5.6
Ethanol	24	5.0	5.0	0.26	1.03	190	0.14	9.4×10^{-12}
	25	9.5	3.7	.16	.95	84	.29	1.7×10^{-11}
	25	9.5	7.9	.29	1.24	330	.12	1.7
	21	9.7	7.0	.38	1.40	360	.20	2.1
	22	9.8	4.8	.18	1.05	120	.21	2.1
	22	9.8	6.3	.23	1.07	190	.15	2.1
	23	10.5	1.4	.07	.92	14	.94	2.1
	23	10.5	2.7	.11	.93	41	.45	2.1
Methanol	26	4.9	4.8	0.19	0.98	270	0.11	5.3×10^{-13}
	24	5.0	6.6	.28	1.13	530	.09	5.7
	26	5.0	7.0	.37	1.31	740	.10	5.4
	21	8.1	7.4	.40	1.52	780	.16	1.1×10^{-12}
	24	18.2	8.9	.26	1.50	650	.16	2.0
	26	18.2	7.9	.38	2.18	840	.30	2.1
	22	18.5	3.8	.09	.97	89	.30	2.4
	23	18.7	8.9	.19	1.16	470	.12	2.1
	25	18.9	8.4	.15	1.06	370	.11	2.0
	23	30.5	10.0	.37	2.58	1030	.30	3.6
	21	32.3	4.7	.07	.99	87	.27	4.3
	22	32.3	11.1	.16	1.34	500	.11	4.1
	19	33.1	11.8	.25	2.06	780	.16	4.7
	22	47.0	12.8	.17	1.65	580	.13	5.9

TABLE IV. - SOLUTION TO MOORE'S EQUATIONS FOR

GIVEN M NUMBER AND DISTORTION PARAMETER

Drag coefficient, C_D, and Reynolds number, Re	M number	Distortion parameter, χ								
		1.01	1.1	1.2	1.5	2.0	2.5	3.0	3.5	4.0
C_D	10^{-8}	----	0.67	0.56	0.54	0.69	0.94	1.26	1.68	2.19
Re		----	59.1	86.9	137	185	220	249	275	299
C_D	10^{-9}	----	0.45	0.37	0.35	0.44	0.58	0.78	1.02	1.31
Re		----	95.2	140	219	295	348	393	432	468
C_D	10^{-10}	----	0.30	0.24	0.22	0.28	0.37	0.48	0.62	0.79
Re		----	153	223	345	468	552	619	679	733
C_D	10^{-11}	0.56	0.19	0.15	0.14	0.18	0.23	0.30	0.38	0.48
Re		62.3	243	352	550	746	872	979	1070	1150
C_D	10^{-12}	0.38	0.13	0.10	0.09	0.11	0.14	0.18	0.23	0.29
Re		101	392	565	875	1170	1370	1530	1670	1800
C_D	10^{-13}	0.25	0.08	0.06	0.06	0.07	0.09	0.11	0.14	0.18
Re		161	618	885	1410	1860	2180	2410	2630	2850

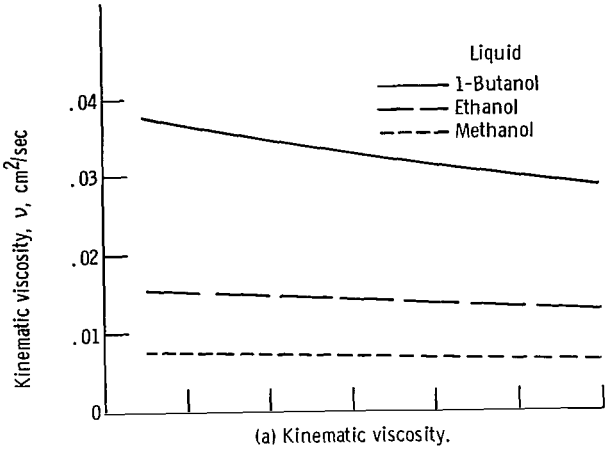

(a) Kinematic viscosity.

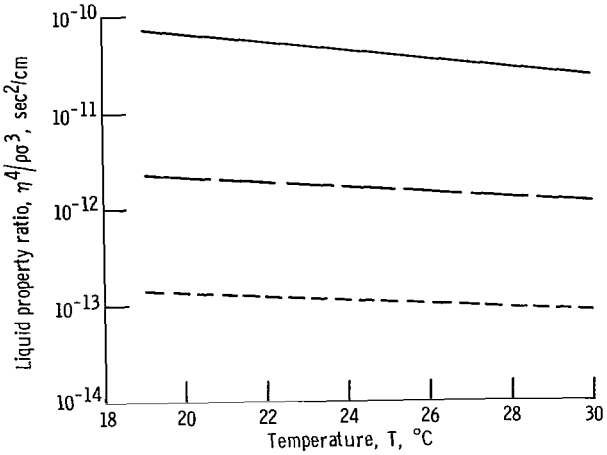

(b) Liquid property ratio.

Figure 1. - Temperature dependence of kinematic viscosity and liquid property ratio.

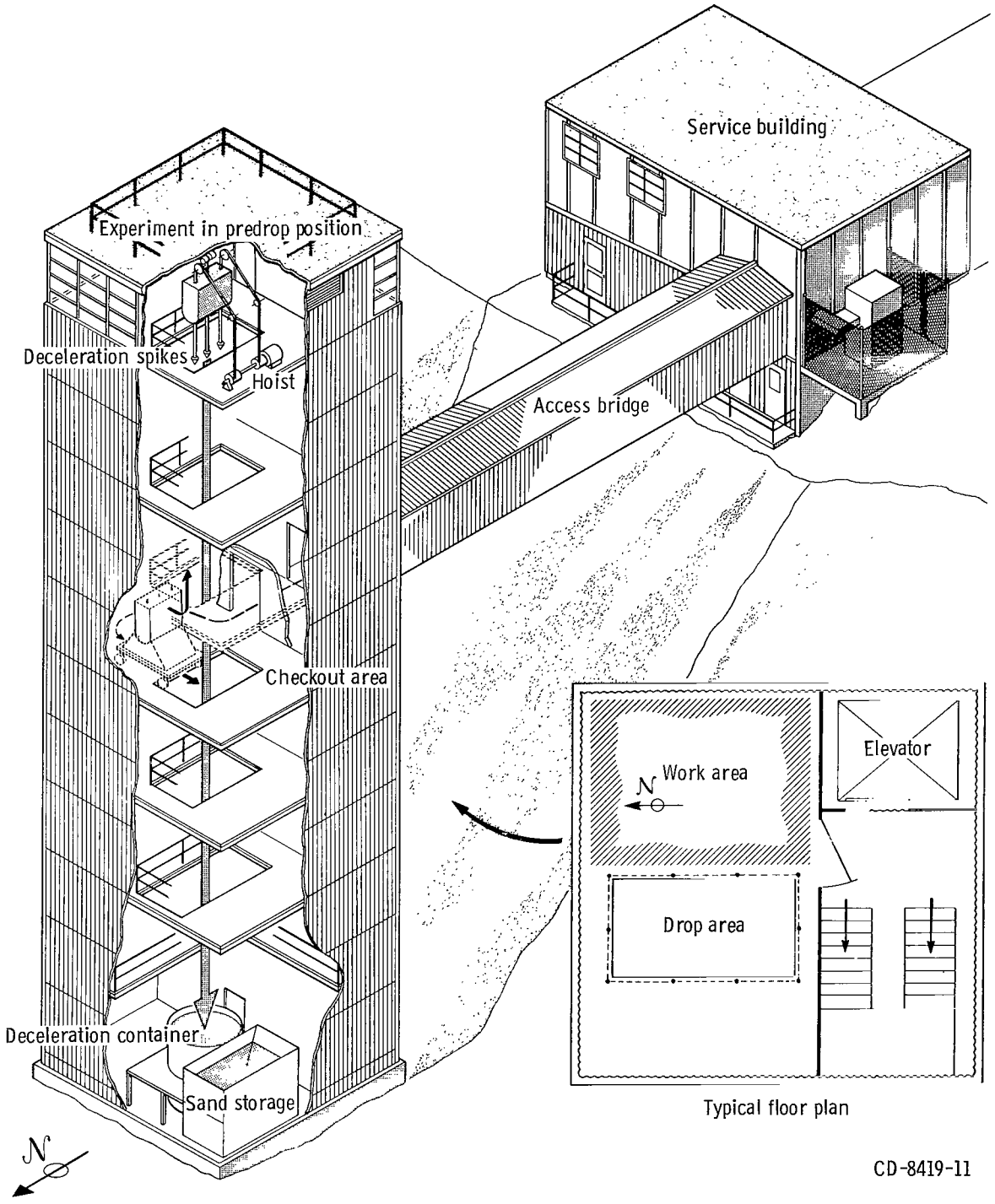

Figure 2. - 2.2-Second Zero-Gravity Facility.

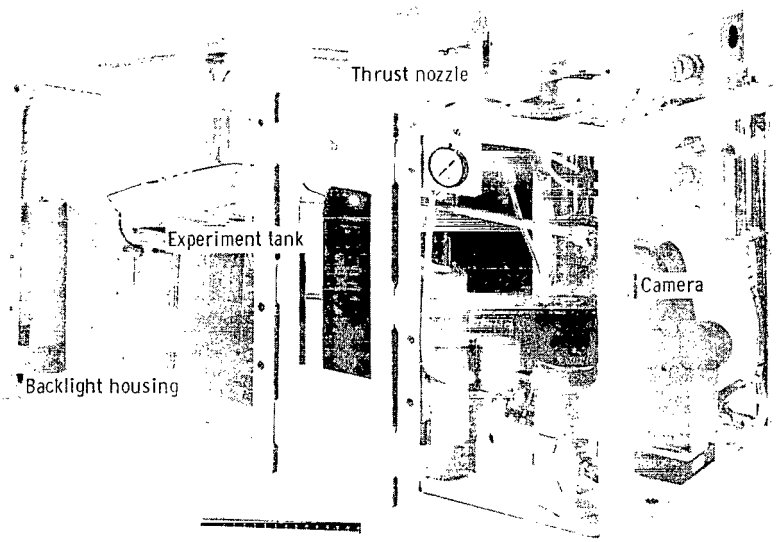

C-67-1502

Figure 3. - Experiment package.

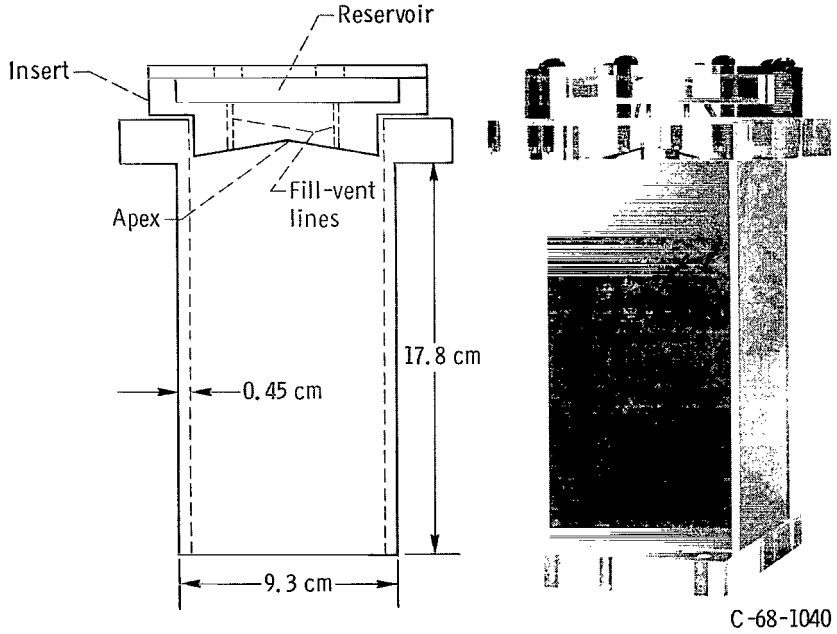

C-68-1040

Figure 4. - Experiment tank used in low-gravity tests.

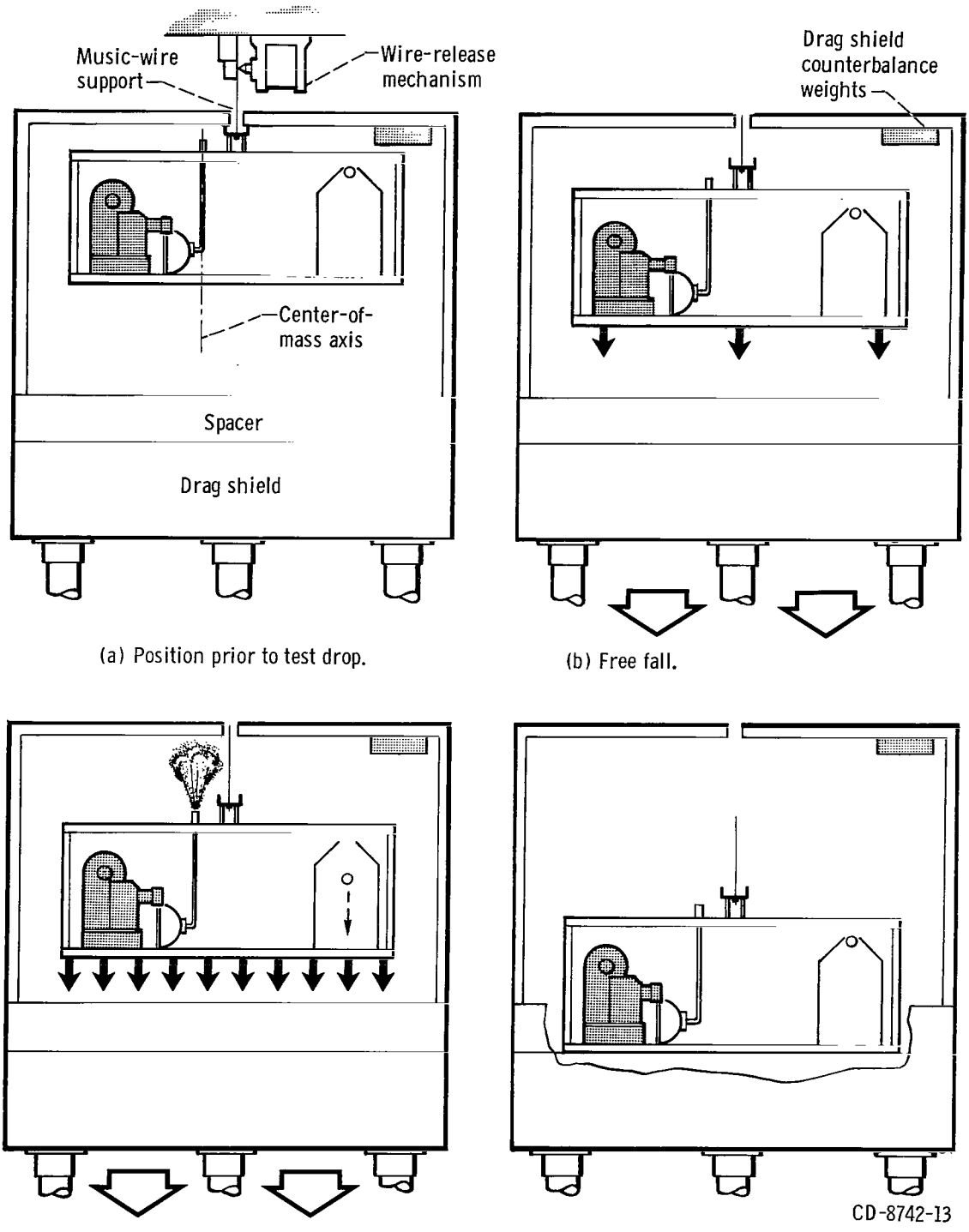

(a) Position prior to test drop.

(b) Free fall.

(c) Application of thrust (low-acceleration field).

(d) Position after test drop.

Figure 5. - Schematic drawing showing sequential position of experiment package and drag shield before, during, and after test drop.

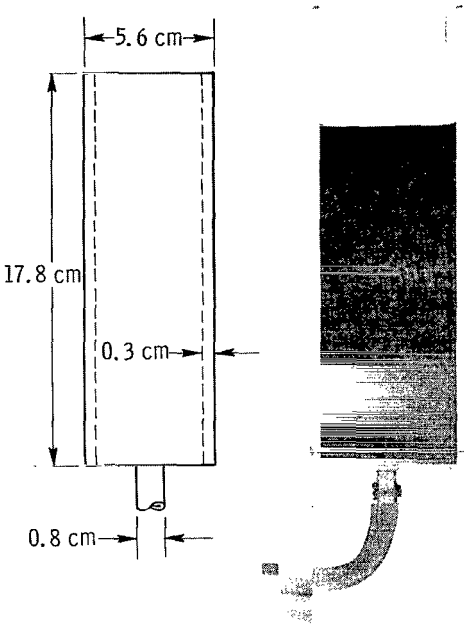

C-68-1041

Figure 6. - Experiment tank used in normal-gravity tests.

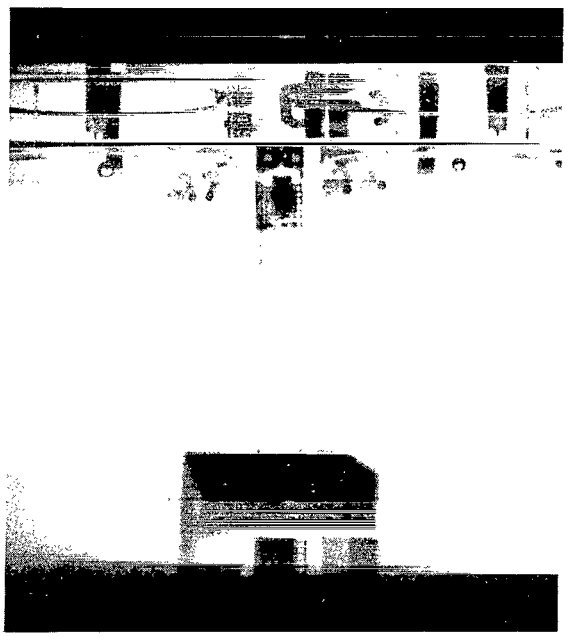

(a) Application of thrust; time, 0.22 second.

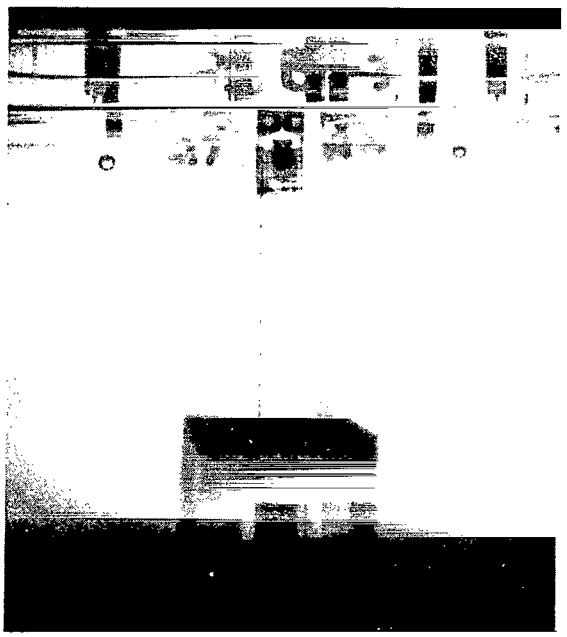

(b) Bubble moving to terminal velocity; time, 0.60 second.

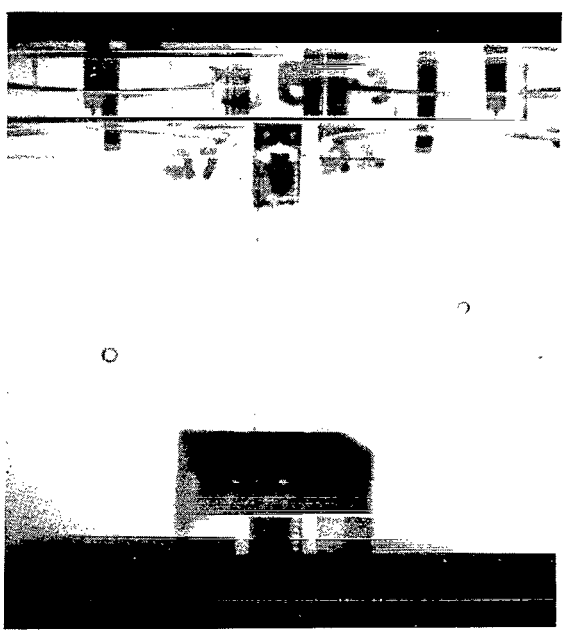

(c) Bubble moving at terminal velocity; time; 1.60 seconds.

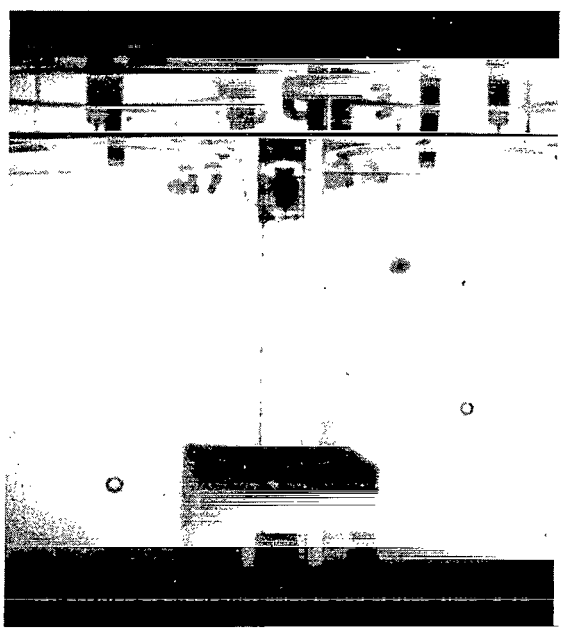

(d) Position of bubble just prior to end of drop; time, 2.16 seconds.

Figure 7. - Typical run sequence.

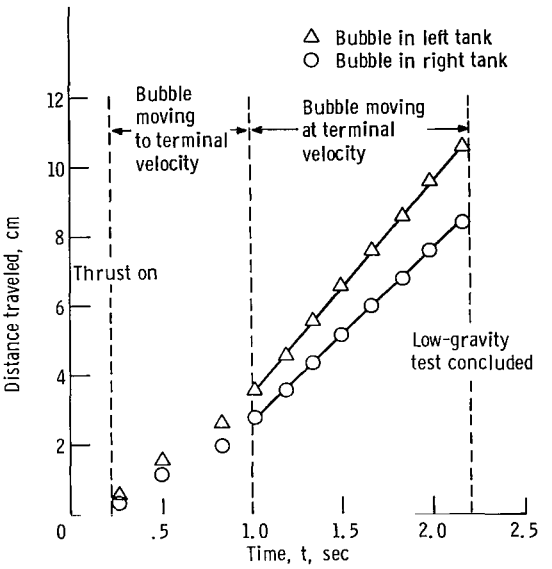

Figure 8. - Data from typical run used in determining bubble terminal velocity. Acceleration, 9.8 centimeters per second squared; test liquid, ethanol.

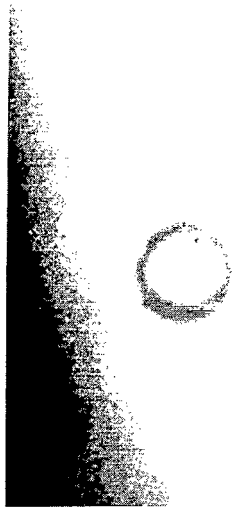

(a) Test liquid, 1-butanol; acceleration, 12.0 centimeter per second squared; equivalent radius, 0.21 centimeter; distortion parameter, 0.94; terminal velocity, 3.7 centimeters per second.

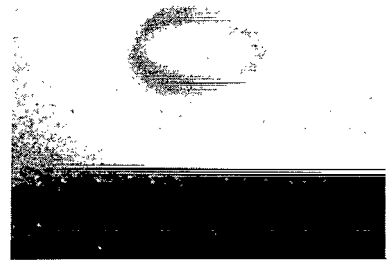

(b) Test liquid, methanol; acceleration, 18.2 centimeters per second squared; equivalent radius, 0.26 centimeter; distortion parameter, 1.50; terminal velocity, 8.9 centimeters per second.

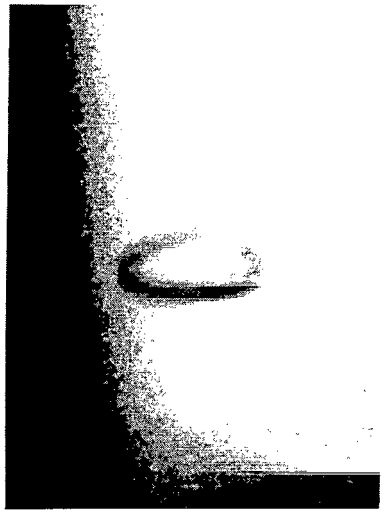

(c) Test liquid, methanol; acceleration, 33.1 centimeters per second squared; equivalent radius, 0.25 centimeter; distortion parameter, 2.06; terminal velocity, 11.8 centimeters per second.

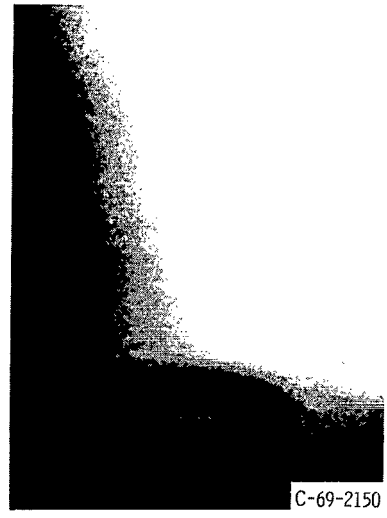

(d) Test liquid, methanol; acceleration, 30.5 centimeters per second squared; equivalent radius, 0.37 centimeter; distortion parameter, 2.58; terminal velocity, 10.0 centimeters per second.

Figure 9. - Distorted bubbles.

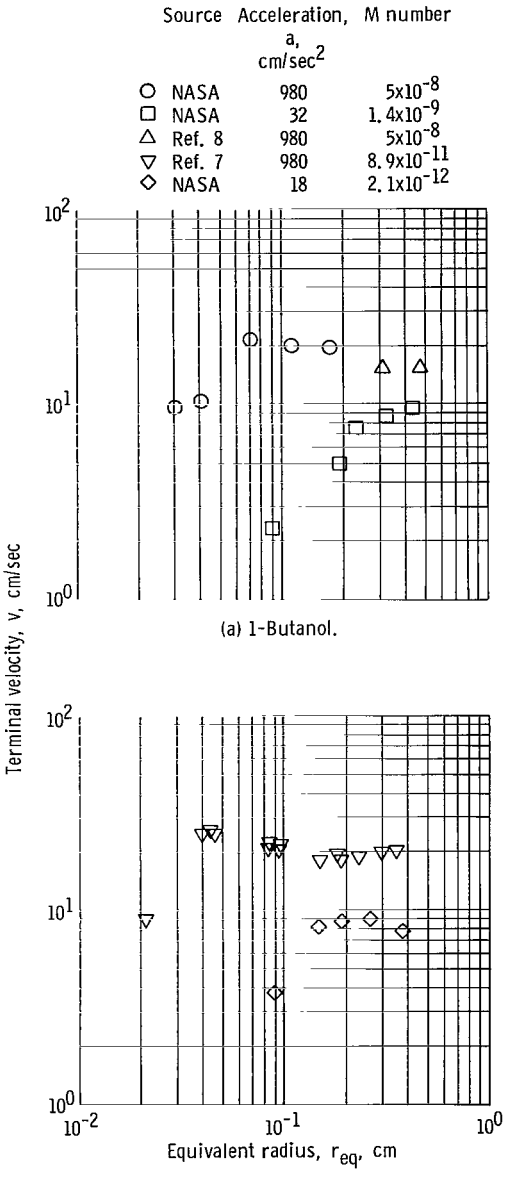

(a) 1-Butanol.

(b) Methanol.

Figure 10. - Effect of gravity on terminal velocity of bubbles.

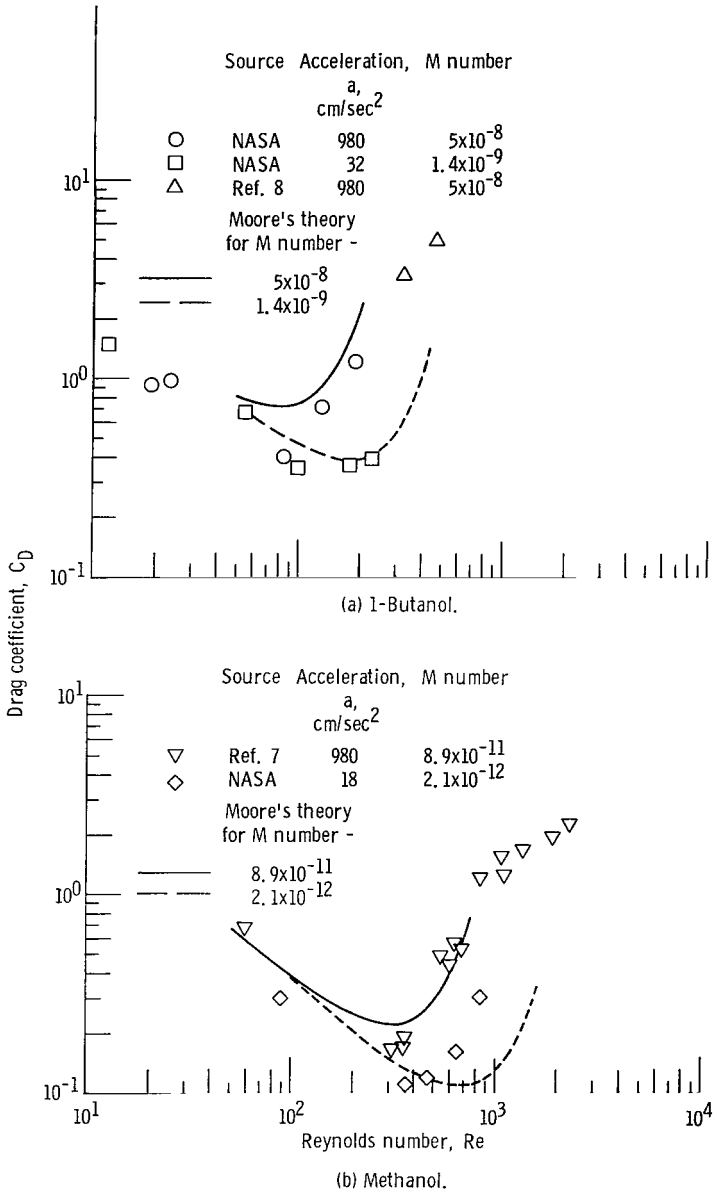

Figure 11. - Effect of gravity on drag coefficient.

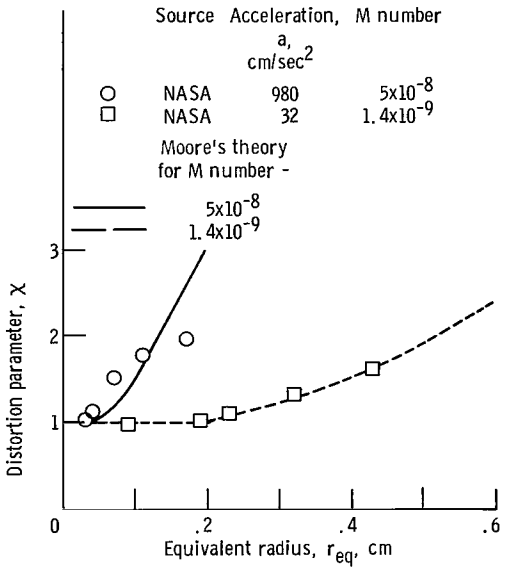

Figure 12. - Typical amount of distorition to an oblate ellipsoid as function of bubble size. Test liquid, 1-butanol.

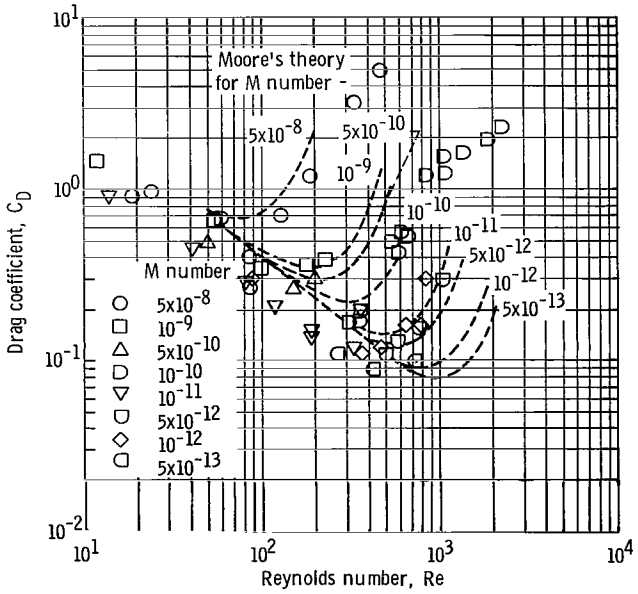

Figure 13. - Experiment results showing M-number trend on drag coefficient for various liquids and gravity fields.

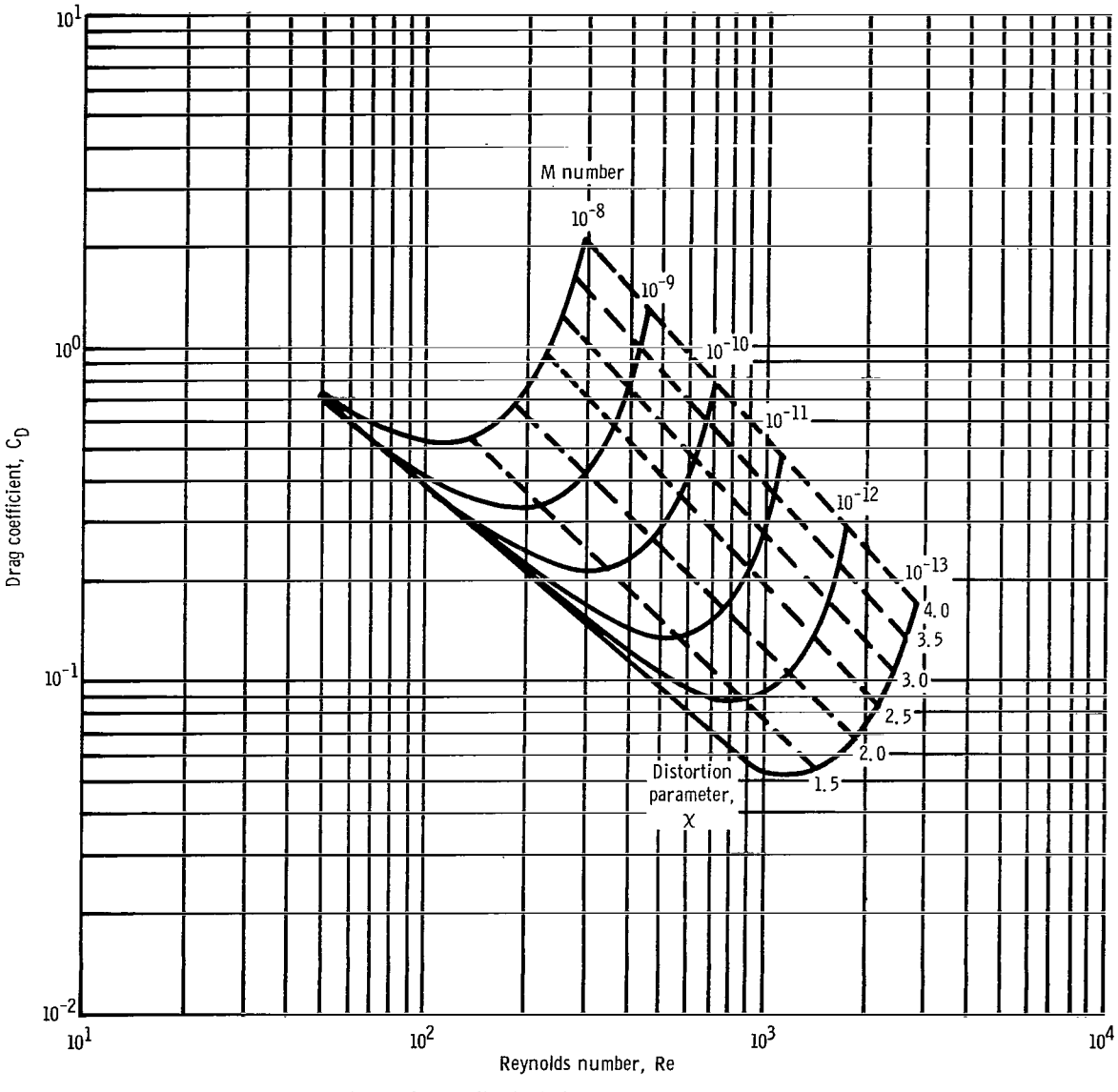

Figure 14. - Family of solutions to Moore's coupled equations.

NASA-Langley, 1969 —— 12 E-5128

NATIONAL AERONAUTICS AND SPACE ADMINISTRATION
WASHINGTON, D. C. 20546
OFFICIAL BUSINESS

FIRST CLASS MAIL

POSTAGE AND FEES PAID
NATIONAL AERONAUTICS AND
SPACE ADMINISTRATION

"The aeronautical and space activities of the United States shall be conducted so as to contribute . . . to the expansion of human knowledge of phenomena in the atmosphere and space. The Administration shall provide for the widest practicable and appropriate dissemination of information concerning its activities and the results thereof."

—NATIONAL AERONAUTICS AND SPACE ACT OF 1958

NASA SCIENTIFIC AND TECHNICAL PUBLICATIONS

TECHNICAL REPORTS: Scientific and technical information considered important, complete, and a lasting contribution to existing knowledge.

TECHNICAL NOTES: Information less broad in scope but nevertheless of importance as a contribution to existing knowledge.

TECHNICAL MEMORANDUMS: Information receiving limited distribution because of preliminary data, security classification, or other reasons.

CONTRACTOR REPORTS: Scientific and technical information generated under a NASA contract or grant and considered an important contribution to existing knowledge.

TECHNICAL TRANSLATIONS: Information published in a foreign language considered to merit NASA distribution in English.

SPECIAL PUBLICATIONS: Information derived from or of value to NASA activities. Publications include conference proceedings, monographs, data compilations, handbooks, sourcebooks, and special bibliographies.

TECHNOLOGY UTILIZATION PUBLICATIONS: Information on technology used by NASA that may be of particular interest in commercial and other non-aerospace applications. Publications include Tech Briefs, Technology Utilization Reports and Notes, and Technology Surveys.

Details on the availability of these publications may be obtained from:

SCIENTIFIC AND TECHNICAL INFORMATION DIVISION

NATIONAL AERONAUTICS AND SPACE ADMINISTRATION

Washington, D.C. 20546